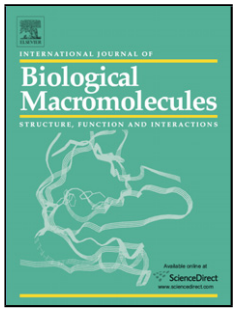

Title: Understanding the structural features of high-amylose maize starch through hydrothermal treatment

Author: Jianing Yang Fengwei Xie Wenqiang Wen Ling Chen Xiaoqin Shang Peng Liu

PII: S0141-8130(15)30214-2
DOI: http://dx.doi.org/doi:10.1016/j.ijbiomac.2015.12.033
Reference: BIOMAC 5629

To appear in: *International Journal of Biological Macromolecules*

Received date: 29-7-2015
Revised date: 25-11-2015
Accepted date: 11-12-2015

Please cite this article as: Jianing Yang, Fengwei Xie, Wenqiang Wen, Ling Chen, Xiaoqin Shang, Peng Liu, Understanding the structural features of high-amylose maize starch through hydrothermal treatment, International Journal of Biological Macromolecules http://dx.doi.org/10.1016/j.ijbiomac.2015.12.033

Understanding the structural features of high-amylose maize starch through hydrothermal treatment

Jianing Yang [a], Fengwei Xie [b,**], Wenqiang Wen [a], Ling Chen [c], Xiaoqin Shang [a], Peng Liu [a,*]

[a] *School of Chemistry and Chemical Engineering, Guangzhou University, Guangzhou 510006, China*

[b] *School of Chemical Engineering, The University of Queensland, Brisbane, Qld 4072, Australia*

[c] *Ministry of Education Engineering Research Center of Starch and Vegetable Protein Processing, Guangdong Province Key Laboratory for Green Processing of Natural Products and Product Safety, College of Light Industry and Food Sciences, South China University of Technology, Guangzhou 510640, China*

[*] Corresponding author: Dr. Peng Liu, School of Chemistry and Chemical Engineering, Guangzhou University, Guangzhou, P.R. China. Tel.: +86 20 3936 6902; fax: +86 20 3936 6903; *Email address:* liu_peng@gzhu.edu.cn (P. Liu).

[**] Corresponding author: Dr. Fengwei Xie, School of Chemical Engineering, The University of Queensland, Brisbane, Australia. Tel.: +61 7 3346 3199; fax: +61 7 3346 3973; *Email address:* f.xie@uq.edu.au, fwhsieh@gmail.com (F. Xie).

Abstract:

In this study, high-amylose starches were hydrothermally-treated and the structural changes were monitored with time (up to 12 h) using scanning electron microscopy (SEM), confocal laser scanning microscopy (CLSM), small-angle X-ray scattering (SAXS), X-ray diffraction (XRD), and differential scanning calorimetry (DSC). When high-amylose starches were treated in boiling water, half-shell-like granules were observed by SEM, which could be due to the first hydrolysis of the granule inner region (CLSM). This initial hydrolysis could also immediately (0.5 h) disrupt the semi-crystalline lamellar regularity (SAXS) and dramatically reduce the crystallinity (XRD); but with prolonged time of hydrothermal treatment (≥ 2 h), might allow the perfection or formation of amylose single helices, resulting in slightly increased crystallinity (XRD and DSC). These results show that the inner region of granules is composed of mainly loosely-packed amylopectin growth rings with semi-crystalline lamellae, which are vulnerable under gelatinization or hydrolysis. In contrast, the periphery is demonstrated to be more compact, possibly composed of amylose and amylopectin helices intertwined with amylose molecules, which require greater energy input (higher temperature) for disintegration.

Keywords: High-amylose starch / Granule structure / Hydrothermal treatment

1. Introduction

Starch is a biopolymer that naturally exists in the form of granules in plants; and the granule is structured in a highly complex way, which has not been fully understood so far [1-3]. Starch has great potentials in a diversity of applications, with some new applications in foods (resistant starch, microporous starch, etc.) [4-5], pharmaceutical materials (drug delivery systems) [6-8], and biodegradable plastics (starch-based materials) [9-11]. A clear understanding of starch structures and how its structures change under different treatments is indispensable for the utilization of starch with desired properties.

It is worth noting that in many applications like those abovementioned, high-amylose starch (a type of starch by genetic modification) is preferably used. High-amylose starch has some special properties, such as its heat resistance [12], which is reflected by high gelatinization temperature and the retainment of granules in boiling water [13-15], and its digestion resistibility [16-17], due to which this starch has been used as resistant starch and in drug delivery systems. In addition, high-amylose starch is especially suitable for producing thermoplastic materials [18-19], because amylose as a linear molecule can provide better mechanical properties resulting from easier formation of crystallites and entanglements. However, when preparing materials, a significant problem would be just the resistance to processing or treatment, because the complete destruction of original starch supramolecular structures is required to form a continuous integrated phase [12-15]. In other words, due to its special structural organization, native high-amylose starch is more resistant to hydrolysis or disintegration by small molecules such as water, enzymes, etc., which negatively impacts on its application.

These particular behaviors of high-amylose starch can hardly be explained by the theories obtained from waxy and regular starches, of which the structural features have been more intensively studied [1-3]. Despite the lower crystallinity, high-amylose starches have a rather compact structure without weak points or voids, which may explain those behaviors to some degree [16-17, 20-21]. Nevertheless, the reason for such a compact granule organization, and how this compact structure is altered during hydrolysis by e.g. water, are not well understood.

There have already been many studies on the compact granule organization of native high-amylose starches [22-27]. Leach and Schoch [25] found that different types of starches showed different degrees of enzyme susceptibility, with waxy maize starch granules being the most susceptible and high-amylose maize starch the least susceptible. It has been proposed that amylose concentrated at the periphery of starch granules could interacts with amylopectin to form a hard shell [28-30], and that amylose could form crystalline structure especially in high-amylose starch granules [31-32], both of which could make the starch granules more compact. In addition, some researchers [33-34] showed that there was no correlation between crystallinity and enzyme susceptibility, and the hydrolysis residues were composed of both amorphous material and B-type crystallites; therefore, they proposed that the distribution of B-type crystallites within the granule and their influence on local granule organization is important. However, to the best of our knowledge, there has been no further exploration on the structural organization of native high-amylose starch granules which account for its compactness.

The current study aims to further explore the structural features of native high-amylose starch, which was done by monitoring the structural changes of high-amylose starch during hydrothermal treatment.

2. Experimental

2.1. Materials and Chemicals

Two varieties of commercially-available maize starches used in this work, Gelose 50 (G50), and Gelose 80 (G80), were supplied by National Starch Pty Ltd. (Lane Cove NSW 2066, Australia). Both of the two starches were chemically unmodified; and their amylose contents were 56.3% and 82.9%, respectively, and their degrees of crystallinity were 31.3% and 28.3%, respectively [35-36], both as measured previously. 8-Aminopyrene-1,3,6-trisulfonic acid trisodium salt (APTS) and sodium cyanoborohydride were purchased from Sigma-Aldrich China (Mainland) (Shanghai, China).

2.2. Hydrothermal treatment of starch

10 g (dry basis) of starch (either G50 or G80) was weighed into distilled water to form 5% suspensions. In a closed environment, these starch suspensions were heated using an oil bath (102 °C) with stirring. Once the suspension reached 50 °C, the time counting was started from zero. From 50 °C (time zero), the temperature could rapidly increase to *ca.* 98 °C within 5 min; afterwards with prolonged time, the temperature could be maintained at *ca.* 98 °C. After specific times (0.5 h, 1 h, 2 h, 4 h, 12 h), one suspension was taken out and immediately quenched in an ice bath for stopping any

further changes. After that, the samples were centrifuged at 5000 rpm for 10 min. The sediments were washed with distilled water for five times, and then freeze-dried for further examinations.

2.3. Scanning electron microscopy (SEM)

The freeze-dried starch samples were adhered to specimen holders using a silver adhesive, and then coated with gold in a vacuum evaporator. The obtained specimens were viewed for their morphologies by a scanning electron microscope (JSM-7001F, Japan Electronics Corporation) at an accelerating voltage of 15 kV.

2.4. Confocal laser scanning microscopy (CLSM)

The starch samples used for CLSM observation were only washed and centrifuged without freeze-drying. APTS was used as the stain and sodium cyanoborohydride were used as the reducing agent. Specifically, 2 mg of the sample was added into a 3 μL freshly-prepared APTS solution (10 mM, with 15% acetic acid solution as the solvent), which was mixed with 3 μL of 1 M sodium cyanoborohydride solution. The mixtures with the starch samples were sealed and kept in a dark place for 15 h at room temperature. Then, the samples were washed with distilled water for five times, and dispersed in a 1:1 water/glycerol solution, before CLSM observation.

Detection of the fluorescence signals from the dye-stained starch samples was carried out using a confocal laser scanning microscope equipped with He/Ne/Ar laser (Nikon Digital Eclipse C1-Plus, Nikon Instruments Inc., Melville, NY, U.S.A.). The detail of objective lens used was Plan Apo VC

60×/1.40 oil. The excitation wavelength was 488 nm. And the emitted light was detected between 500 and 535 nm [37]. The resolution of generated images was 512×512 pixels. The magnification of photos was determined by the product of eye lens and objective lens (10×60). During image acquisition, each line was scanned for four times and averaged in order to reduce noise.

2.5. Small-angle X-ray scattering (SAXS) analysis

SAXS experiments were performed using an SAXSess system (Anton-Paar GmbH, Austria) equipped with a PW3830 X-ray generator (PANalytical B.V., Netherlands), operated at 50 mA and 40 kV, using Cu Kα radiation with a wavelength of 0.1542 nm as the X-ray source. The moisture content of freeze-dried starch samples were adjusted to 50% by adding a certain amount of water, and equilibrated at 20 °C for 24 h, before the detection. The sample was filled into a sample cell and measured for 10 min. The data, recorded using an image plate, were collected by the IP Reader software program with a PerkinElmer® Storage Phosphor System. All data were normalized, and the background intensity and smeared intensity were removed using the SAXS Quant 3.0 software program for further analysis.

2.6. X-ray diffraction (XRD) analysis

XRD analysis was performed with an Xpert PRO diffractometer (PANalytical B.V., Netherlands), operated at 40 mA and 40 kV, using Cu Kα radiation with a wavelength of 0.1542 nm as the X-ray source. The scanning was carried out with the diffraction angle (2θ) from 5° to 50° with a scanning speed

of 10°/min and a scanning step of 0.033°. The samples were equilibrated at 40 °C for 24 h and the moisture content of all the samples was about 10% before analysis.

The degrees of crystallinity of the samples were quantitatively estimated according to a previous study [36]. Specifically, a smooth curve connected with the peak baseline was computer-plotted on the diffraction. The area above the smooth curve was regarded as the crystalline portion, while the lower area between the smooth curve and a linear baseline that connected the three points at 4°, 6°, and 28° was taken as the amorphous portion. The upper diffraction peak area and the total diffraction area were integrated by MDI Jade 6. The ratio of upper area to total diffraction area was taken as the degree of crystallinity.

2.7. Differential scanning calorimetry (DSC)

A PerkinElmer® Diamond DSC with an internal coolant (Intercooler IP) and nitrogen purge gas was used in the experimental work. The melting points and enthalpies of indium and zinc were used for temperature and heat capacity calibration. A high-pressure stainless steel pan (PE No. B0182901) with a gold-plated copper seal (PE No. 042-191758) was used to keep the moisture content constant during DSC measurements. The starch samples, with a moisture content of *ca.* 50%, were prepared in sealed glass vials, which were kept at 20 °C for 24 h before measurement. With this moisture content, the DSC endothermic features could be clearly illustrated containing separated characteristic peaks of gelatinization (G) and the phase transition of amylose-lipid complexes (M2) [13]). For each measurement, about 10 mg of the sample in the pan was used, which was scanned from 30 to 140 °C. A

slow heating rate of 5 °C/min was used for minimizing any temperature lag due to the large mass of the steel pan [38]. The onset temperature (T_o), peak temperature (T_p) and the enthalpy (ΔH) of starch thermal transitions were recorded. The enthalpy was calculated based on the weight of dry starch. The results were presented as the average of three replicates.

3. Results and discussions

3.1. Morphological changes of high-amylose starch after hydrothermal treatment

Fig. 1 shows the morphological images of G50 and G80 before and after hydrothermal treatment for 30 min by SEM. Both native G50 and G80 granules displayed a nearly spherical shape with smooth surface. For some of the granules, a small depression on the surface could be clearly identified. After hydrothermal treatment for 30 min, hollowed or half-shell-like granules could be formed for both G50 and G80, and almost all granules turned into this morphology. The diameter of the pit was about 4~5 μm for G50 starch, nearly a half of the whole granule; and 2~3 μm for G80 starch, approximately 1/3 of the whole granule. These hollowed or half-shell-like granules have also been observed before for other types of high-amylose starch under enzymatic treatment conditions [32].

As these hollowed or half-shell-like granules might be formed by the drying and grinding process before the SEM measurement, CLSM was further used for morphological observation. For the CLSM measurements, the samples were dyed directly after hydrothermal treatment, and the images are shown in Fig. 2. It could be seen that both G50 and G80 samples dyed with APTS showed strong fluorescence. Previous studies have shown that starch with higher amylose content could display stronger fluorescent

intensity [20-21]. This is because amylose has a lower molecular weight than amylopectin and contains a much higher mole ratio of reducing ends per anhydrous glucose residues, resulting in a higher by-weight labeling of amylose [39].

It can be seen from Fig. 2 that, for some granules, the periphery showed strong fluorescence whereas the inner region was predominantly dark. This could also be verified by the CLSM images of these granules viewed at gradually varied focusing depth (images not shown here). Taking into consideration of the SEM results previously discussed, the dark inner region of granule under CLSM could be due to the less compact structure in the granule, which might have been gelatinized or hydrolyzed to some degree. It is plausible that starch molecules around the hilum were promptly gelatinized and hydrolyzed because the starch molecules around the hilum were loosely packed and had less amylose [29, 30, 32]. The remaining structure, after 0.5 h of hydrothermal treatment, looked intact and smooth without showing any growth rings and channels, suggesting its stronger resistance to hydrothermal treatment. However, as the half-shell-like granules (shown in SEM) could not be seen from CLSM images, they were proposed to be formed by the drying process (for SEM observation) after the initial hydrolysis of the inner region (which made the outer layer partly collapse, forming a pit).

3.2. Structural changes of high-amylose starch after hydrothermal treatment

Fig. 3 shows the SAXS results of G50 and G80 before and after hydrothermal treatment for 30 min. It is apparent that there was a peak positioned at around $q = 0.6$ nm^{-1}, which corresponds to the average repeat distance ($d = 2\pi/q$) of the semi-crystalline lamellae in native high-amylose starch granules being

10 nm [40]. The semi-crystalline lamellae in 10 nm are important information, as they are formed by the periodic appearance of the branched points and the branched chains of amylopectin, and contribute to the structures of blocklets and growth rings [41]. This SAXS characteristic peak did not exist for the samples after treatment for 0.5 h. This suggested that the first 0.5 h of treatment was enough to disrupt the starch lamellar structure (regularity).

Fig. 4(a) and (b) show the XRD curves of G50 and G80 before and after hydrothermal treatment for different time periods. It can be seen that native G50 showed the strongest diffraction peaks at 2θ of around 17°, with a few smaller peaks at 2θ of around 5°, 14.5°, 15°, 20°, 22°, 23°, 26°, 30.5°, and 34°, which were indicative of B-type crystalline structure [42-43]. After treatment for 0.5 h, these peaks were largely depressed, with some peaks (5° and 14.5°) becoming invisible. However, with a longer time (≥ 2 h), the peaks at 20° and 22° were seen to be strengthened. Specifically, the peak became much sharper at 12 h than at 0.5 h; while the peak at 22°, which almost disappeared after 0.5 h of hydrothermal treatment, emerged again on the curves for 4 h and 12 h. These peaks at 20° and 22° are characteristics of V_H-type crystalline structure, a single-helical amylose structure (similar to that formed by amylose–lipid helical complexes) [44]. On the other hand, native G80 also displayed B-type crystalline structure and very similar evolution of the XRD pattern as a result of hydrothermal treatment could be seen. The changes in crystallinity for G50 and G80 can be better illustrated in Fig. 4(c). It can be seen that after 0.5 h of treatment, the crystallinity for both G50 and G80 rapidly decreased, which maintained at a similar low value until 2 h. Along with the results of SEM (Fig. 1), CLMS (Fig. 2), and SAXS (Fig. 3), the crystallinity change here suggested that hydrothermal treatment

firstly disrupted the granule inner region, which was mostly crystalline. After that, the crystallinity increased slightly with time (2–12 h), which could be considered as an annealing process.

Fig. 5 and Table 1 show the DSC endothermic results of the two starches before and after hydrothermal treatment for different time periods. It can be seen that both native G50 and G80 had a major transition between 70 °C and 90 °C, immediately followed by a gentler peak between 100 °C and 120 °C. According to previous studies, the first peak, normally considered as the gelatinization peak, represents the transition from smectic to nematic phase regarding the alignment of amylopectin double helices (G peak) [13-14], which is usually along with the helix-coil transition associated with the unwinding of amylopectin double helices (M1 peak) when abundant water exists; and the second peak is considered as the thermal transition associated with the unwinding of amylose single helices (M2 peak) [45-48].

For G50 after hydrothermal treatment for 0.5–2 h, only the M2 peak at the higher temperature was shown, which corresponds to the SAXS results showing the disappearance of semi-crystalline lamellae after hydrothermal treatment (so the absence of the smectic-to-nematic transition (G) in DSC). Besides, both T_o and T_p of the M peak became gradually higher, and so did ΔH. For G80, the similar evolution of thermal transitions with time of hydrothermal treatment was also observed. The increasing in ΔH suggested an increase in the relative portion of amylose helices in the granule remains; and the higher temperature of M peak could be due to an annealing process (for greater perfection of amylose single helices) induced by hydrothermal treatment. These results are in agreement with the XRD analysis.

3.3. Further discussion regarding the structural features of high-amylose starch

While the structures of other types of starch have been intensively studies, much less understanding of the structure of high-amylose starch has been acquired. Native high-amylose starch has a compact granule structure and behaves distinctly. It shows greater resistance to thermal [13-14], mechanical [15, 19], acidic [20-21], and enzymatic treatments [25]. While the reason for this was normally ascribed to the more compact structure of high-amylose starch granules, why the granule is compact and maintains a better integrity has not been well elaborated. It is widely accepted that amylopectin is responsible for the supramolecular structure of granules [1-3]. And the most accepted model of amylose location in starch granules is as individual, radially oriented chains randomly distributed and could disrupt the structural order within the amylopectin crystallites [1]. Research has also suggested that amylose could form double helical crystallites in high-amylose starch [31-32]. Therefore, it could be rather considered here that the more compact periphery is composed by both amylopectin and amylose helical crystallites (with the amylose helices longer than amylopectin helices [32]) intertwined with amylose molecules. This is proposed considering that amylose is more flexible and has a much greater length than that of double helices (5–6 nm) formed by amylopectin branches [3], and that amylose is more concentrated at the periphery in maize starch [2]. Fig. 6 is a speculated schematic regarding the supramolecular structure at the periphery of maize starch granule.

In contrast, in the starch granule center, the parts adjacent to the hilum are more crystalline with regular lamellar periodicity, but have a loosely packed structure [2], probably because there is weak

tangential (regarding the granule) force for the association of parallel helices. Therefore, gelatinization or hydrolysis starts from the granule inner region, creating hollowed granules.

4. Conclusions

By hydrothermal treatment, the current study further explores the special structural organization of high-amylose starch granules responsible for their resistance to gelatinization or hydrolysis. SEM and CLSM images show that the hydrolysis mostly started from the inner region, generating hollowed granules. This initial hydrolysis could disrupt the semi-crystalline lamellar structure as shown by SAXS and dramatically reduce the crystallinity as demonstrated by DSC and XRD. According to the literature and the observation here, it is proposed that while the inner region of granules is composed of mainly loosely-packed amylopectin growth rings with semicrystalline lamella, which are susceptible to hydrolysis or gelatinization, the more compact periphery is composed by both amylopectin and amylose helical crystallites intertwined with amylose molecules. We hope the speculated model of the granule periphery here could attract further research for high-amylose starch structure, which is highly important in understanding the mechanisms of different treatment processes for high-amylase starch, for the preparation of materials and resistant starch for example.

Acknowledgments

The research leading to these results has received funding from the National Natural Science Foundation of China (NSFC) (Project Nos. 21106023 and 31271942), the “Science and Technology

Projects supported by Guangzhou Education Bureau" (Project No. 1201410965), and the "Training Programs of Innovation and Entrepreneurship for Undergraduates supported by Guangzhou University" (Project No. 201511078034). Besides, the authors also thank for the financial support provided by the Ministry of Education Engineering Research Center of Starch and Vegetable Protein Processing, South China University of Technology, Guangzhou, 510640, China.

References

[1] S. Pérez, P.M.Baldwin, D.J.Gallant, Structural features of starch granules I, in: B. James, W. Roy, (Eds.), Starch (Third Edition), Academic Press, San Diego, 2009, pp 149-192.

[2] J.L. Jane, Structural features of starch granules II. In: B. James, W. Roy, (Eds.), Starch (Third Edition), Academic Press, San Diego, 2009, pp 193-236.

[3] S. Pérez, E. Bertoft, The molecular structures of starch components and their contribution to the architecture of starch granules: A comprehensive review, Starch/Stärke. 62 (2010) 389-420.

[4] S. Jobling, Improving starch for food and industrial applications, Curr. Opin. Plant. Biol. 7 (2004) 210-218.

[5] E. Fuentes-Zaragoza, M.J. Riquelme-Navarrete, E. Sánchez-Zapata, J.A. Pérez-Álvarez, Resistant starch as functional ingredient: A review, Food. Res. Int. 43 (2010) 931-942.

[6] A. Rodrigues, M. Emeje, Recent applications of starch derivatives in nanodrug delivery, Carbohydr. Polym. 87 (2012) 987-994.

[7] H. Pu, L. Chen, X. Li, F. Xie, L. Yu, L. Li, An oral colon-targeting controlled release system based on resistant starch acetate: synthetization, characterization, and preparation of film-coating pellets, J. Agric. Food Chem. 59 (2011) 5738-5745.

[8] X.Li, P.Zhang, L.Chen, F.Xie, L.Li, B.Li, ,Structure and colon-targeted releasing property of resistant octenyl succinate starch, Food. Res. Int. 47 (2012) 246-252.

[9] H.Liu, F.Xie, L.Yu, L.Chen, L.Li, Thermal processing of starch-based polymers, Prog. Polym. Sci. 34 (2009) 1348-1368.

[10] F.Xie, P.J.Halley, L.Avérous, Rheology to understand and optimize processibility, structures and properties of starch polymeric materials, Prog. Polym. Sci. 37 (2012) 595-623.

[11] F.Xie, E.Pollet, P. J.Halley, L.Avérous, Starch-based nano-biocomposites, Prog. Polym. Sci. 38 (2013) 1590-1628.

[12] W.S. Ratnayake, D.S. Jackson, Starch gelatinization. In Advances, in: S.L. Taylor, (Ed.), Food and Nutrition Research, Academic Press, Amsterdam, 2008, pp 221-268.

[13] H. Liu, L. Yu, F. Xie, L .Chen, Gelatinization of cornstarch with different amylose/amylopectin content, Carbohydr. Polym. 65 (2006) 357-363.

[14] P. Liu, F. Xie, M. Li, X. Liu, L. Yu, P.J. Halley, L. Chen, Phase transitions of maize starches with different amylose contents in glycerol–water systems, Carbohydr. Polym. 85 (2011) 180-187.

[15] J. Wang, L.Yu, F.Xie, L.Chen, X. Li, H. Liu, Rheological properties and phase transition of cornstarches with different amylose/amylopectin ratios under shear stress, Starch/Stärke. 62 (2010) 667-675.

[16] M.G. Sajilata, R.S. Singhal, P.R. Kulkarni, Resistant Starch–A Review, Compr. Rev. Food Sci.F. 5 (2006) 1-17.

[17] H.X. Jiang, J.L. Jane, Type 2 Resistant Starch in High-Amylose Maize Starch and its Development, in: Y.C. Shi, C.C. Maningat, (Eds.), Resistant starch sources, applications and health benefits, John Wiley & Sons Ltd, Chichester, 2013 pp 23-42

[18] W.C. Liu, P.J. Halley, R.G. Gilbert, Mechanism of Degradation of Starch, a Highly Branched Polymer, during Extrusion, Macromolecules. 43 (2010) 2855-2864.

[19] M. Li, P. Liu, W. Zou, L. Yu, F. Xie, H. Pu, H. Liu, L. Chen, Extrusion processing and characterization of edible starch films with different amylose contents, J. Food. Eng. 106 (2011) 95-101.

[20] P. Chen, L.Yu, G. Simon, E. Petinakis, K. Dean, L. Chen, Morphologies and microstructures of cornstarches with different amylose–amylopectin ratios studied by confocal laser scanning microscope, J. Cereal Sci. 50 (2009) 241-247.

[21] P. Chen, L.Yu, G.P. Simon, X. Liu, K. Dean, L. Chen, Internal structures and phase-transitions of starch granules during gelatinization, Carbohydr. Polym. 83 (2011) 1975-1983.

[22] A.W. MacGregor, D.L. Ballance, Hydrolysis of Large and Small Starch Granules from Normal and Waxy Barley Cultivars by Alpha-Amylases from Barley Malt, Cereal Chem. 57 (1980) 397-402.

[23] S. Schwimmer, The role of maltase in the enzymolysis of raw starch, J. Biol. Chem.161 (1945) 219-234.

[24] Z. Nikuni, R.L.Whistler, Unusual structure in corn starch granules, J. Biochem. 44 (1957) 227-231.

[25] H.W. Leach, T.J. Schoch, Structure of the Starch Granule. II. Action of Various Amylases on Granular Starches, Cereal. Chem. 38 (1961) 34-46.

[26] H. Fuwa, D.V. Glover, Y. Sugimoto, M.J. Tanaka, Comparative susceptibility to amylases of starch granules of several single endosperm mutants representative of floury-opaque,

starch-deficient, and modified starch types and their double-mutant combinations with opaque-2 in four inbred lines of maize, Nutr. Sci. Vitaminol. 24 (1978) 437-448.

[27] W. Helbert, M. Schülein, B. Henrissat, Electron microscopic investigation of the diffusion of Bacillus licheniformis alpha-amylase into corn starch granules, Int. J. Biol. Macromol. 19 (1996) 165-169.

[28] M.R. Debet, M.J. Gidley,Why Do Gelatinized Starch Granules Not Dissolve Completely? Roles for Amylose, Protein, and Lipid in Granule "Ghost" Integrity, J. Agric. Food Chem. 55 (2007) 4752-4760.

[29] J.L. Jane, J.J. Shen, Internal structure of the potato starch granule revealed by chemical gelatinization, Carbohydr. Res. 247 (1993) 279-290.

[30] D.D. Pan, J.L. Jane, Internal structure of normal maize starch granules revealed by chemical surface gelatinization, Biomacromolecules. 1 (2000) 126-132.

[31] Y.C. Shi, T.Capitani, P. Trzasko, R. Jeffcoat, Molecular Structure of a Low-Amylopectin Starch and Other High-Amylose Maize Starches, J. Cereal Sci. 27 (1998) 289-299.

[32] H. Jiang, M. Campbell, M. Blanco, J.L. Jane, Characterization of maize amylose-extender (ae) mutant starches: Part II. Structures and properties of starch residues remaining after enzymatic hydrolysis at boiling-water temperature, Carbohydr. Polym. 80 (2010) 1-12.

[33] C. Gérard, P. Colonna, A. Buléon, V. Planchot, Amylolysis of maize mutant starches, J. Sci. Food Agric. 81 (2001) 1281-1287.

[34] A. Evans, D.B.Thompson, Resistance to α-Amylase Digestion in Four Native High-Amylose Maize Starches, Cereal Chem. 81 (2004) 31-37.

[35] I. Tan, B.M. Flanagan, P.J. Halley, A.K. Whittaker, M.J. Gidley, A method for estimating the nature and relative proportions of amorphous, single, and double-helical components in starch granules by C-13 CP/MAS NMR, Biomacromolecules. 8 (2007) 885-891.

[36] H. Liu, L. Yu, G. Simon, X. Zhang, K. Dean, L. Chen, Effect of annealing and pressure on microstructure of cornstarches with different amylose/amylopectin ratios, Carbohydr. Res. 344 (2009) 350-354.

[37] M.A. Glaring, C.B. Koch, A. Blennow, Genotype-Specific Spatial Distribution of Starch Molecules in the Starch Granule: A Combined CLSM and SEM Approach. Biomacromolecules. 7 (2006) 2310-2320.

[38] L.Yu, G. Christie, Measurement of thermal transitions using differential scanning calorimetry, Carbohydr. Polym. 46 (2001) 179-184.

[39] A. Blennow, M. Hansen, A. Schulz, K. Jørgensen, A.M. Donald, J. Sanderson, The molecular deposition of transgenically modified starch in the starch granule as imaged by functional microscopy, J. Struct. Biol. 143 (2003) 229-241.

[40] V.I. Kiseleva, A.V. Krivandin, J. Fornal, W. Blaszczak, T. Jelinski, V.P. Yuryev, Annealing of normal and mutant wheat starches. LM, SEM, DSC, and SAXS studies. Carbohydr Res, 2005. 340(1): p. 75-83.

[41] M.A. Glaring, C.B. Koch, A. Blennow, Microscopy of starch: Evidence of a new level of granule organization.[J]. Carbohydrate Polymer, 1997, 32: 177-191.

[42] A. Lopez-Rubio, B.M. Flanagan, E.P. Gilbert, M.J. Gidley, A novel approach for calculating starch crystallinity and its correlation with double helix content: A combined XRD and NMR study, Biopolymers. 89 (2008) 761-768.

[43] N.W.H. Cheetham, L. Tao, Variation in crystalline type with amylose content in maize starch granules: an X-ray powder diffraction study, Carbohydr. Polym. 36 (1998) 277-284.

[44] J.J.G. van Soest, S.H.D. Hulleman, D. de Wit, J.F.G. Vliegenthart, Crystallinity in starch bioplastics, Ind. Crops. Prod. 5 (1996) 11-22.

[45] T.A. Waigh, M.J. Gidley, B.U. Komanshek, A.M. Donald, The phase transformations in starch during gelatinisation: a liquid crystalline approach, Carbohydr. Res. 328 (2000) 165-176.

[46] G. Jovanovich, M.C. Añón, Amylose-lipid complex dissociation. A study of the kinetic parameters, Biopolymers. 49 (1999) 81-89.

[47] S. Raphaelides, J. Karkalas, Thermal dissociation of amylose-fatty acid complexes, Carbohydr. Res. 172 (1988) 65-82.

[48] C.G. Biladeris, C.M. Page, L. Slade, R.R. Sirett, Thermal behavior of amylose-lipid complexes, Carbohydr. Polym. 5 (1985) 367-389.

Figure captions

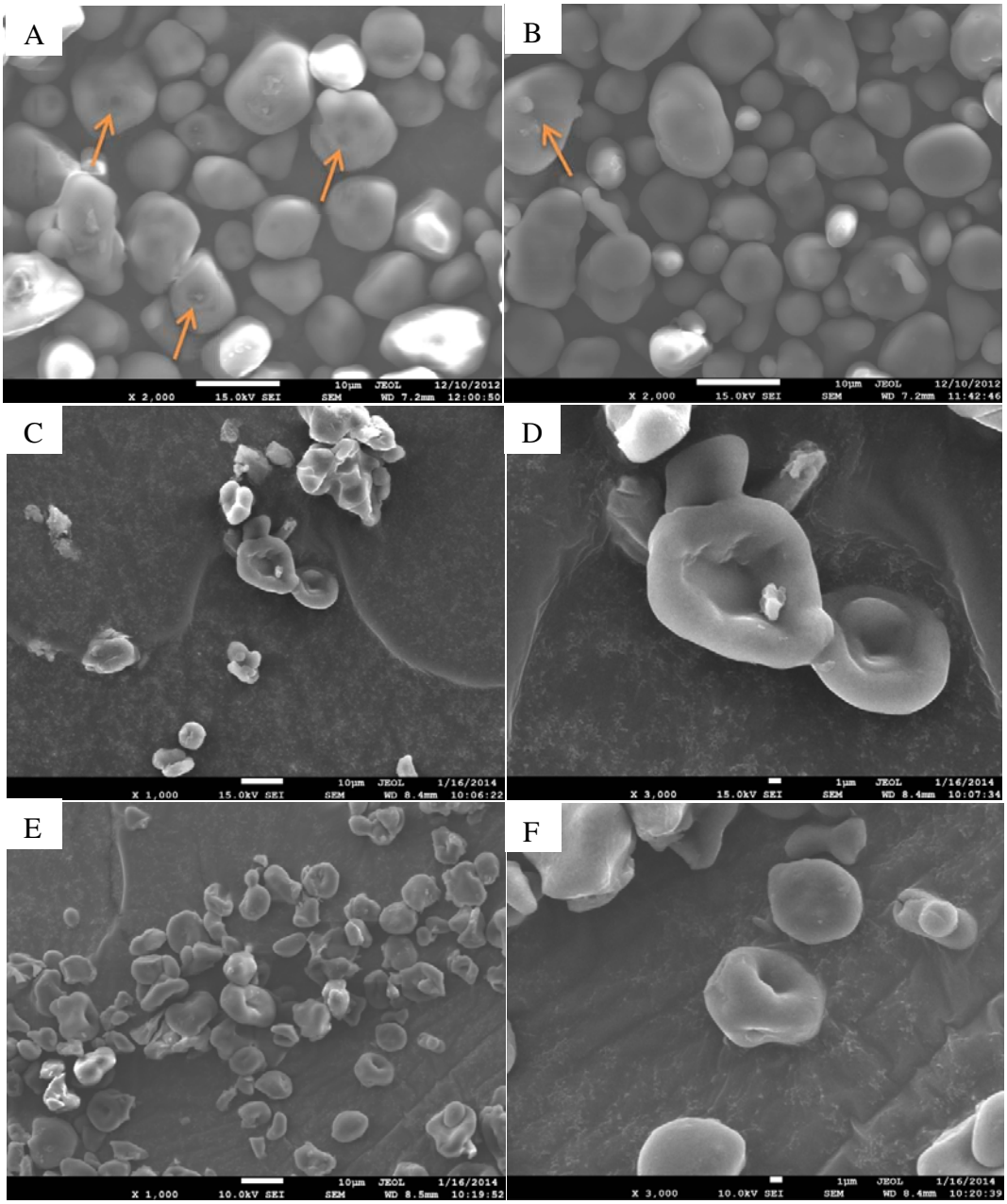

Fig. 1

Yang et al.
International Journal of Biological Macromolecules

Fig. 1. Morphology of high-amylose starch granules by SEM. (A) and (B) were native G50 and G80 starch granules respectively (magnification: ×2000); (C) and (E) were G50 and G80 after hydrothermal treatment for 0.5 h, respectively (magnification: ×1000); (D) and (F) were part

of (C) and (E) magnified respectively (magnification: ×3000). The arrows indicate the small depressions on the granule surfaces of native starches.

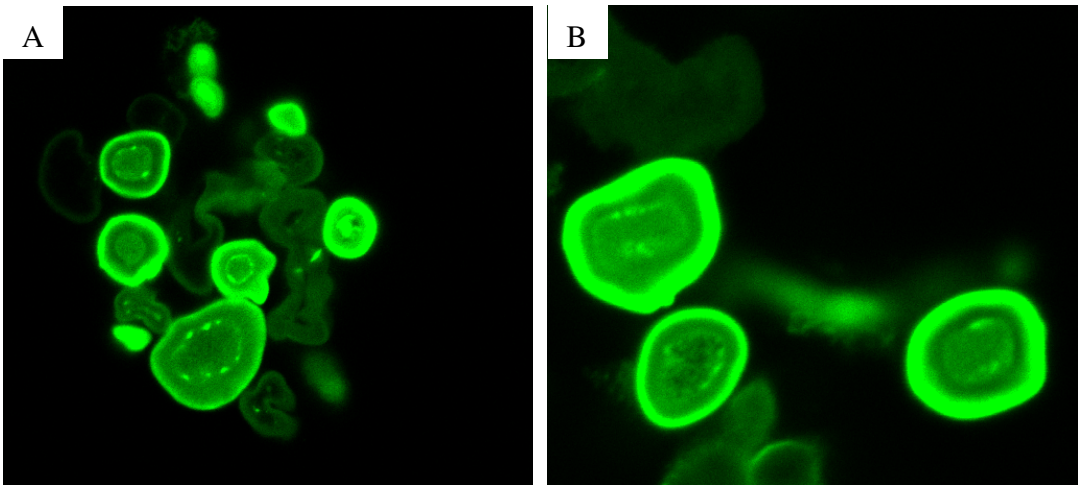

Fig. 2

Yang et al.

International Journal of Biological Macromolecules

Fig. 2. CLSM images of high-amylose starch granules (A: G50; B: G80) after hydrothermal treatment for 0.5 h (magnification: ×600).

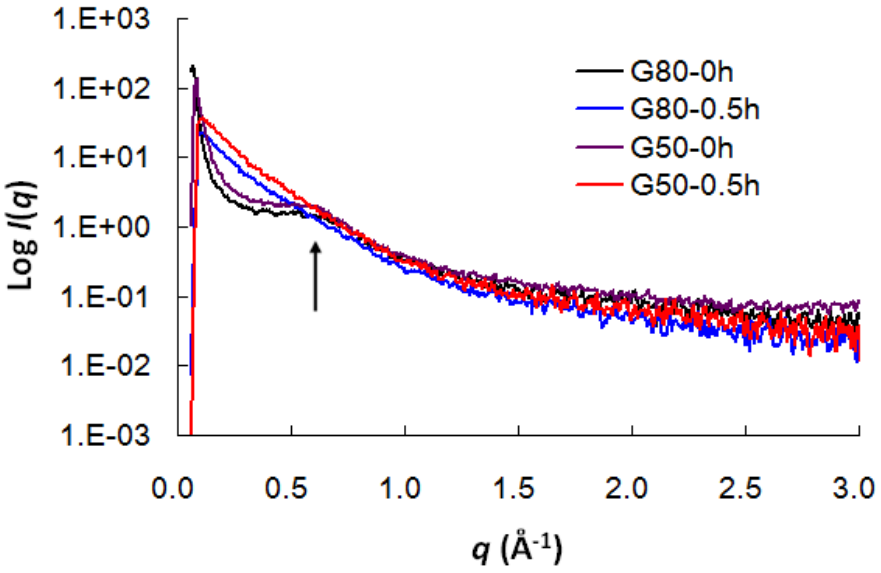

Fig. 3

Yang et al.

International Journal of Biological Macromolecules

Fig. 3. SAXS results of G50 and G80 after hydrothermal treatment for 0 h and 0.5 h. The arrow pointed to the peaks of *q*, which is for calculating the repeat distance of starch semi-crystalline lamellar structure.

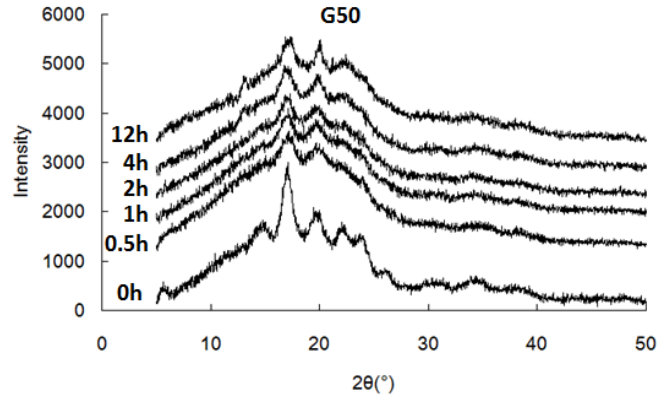

A

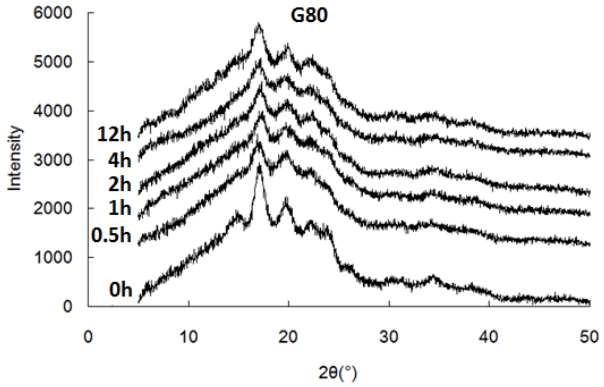

B

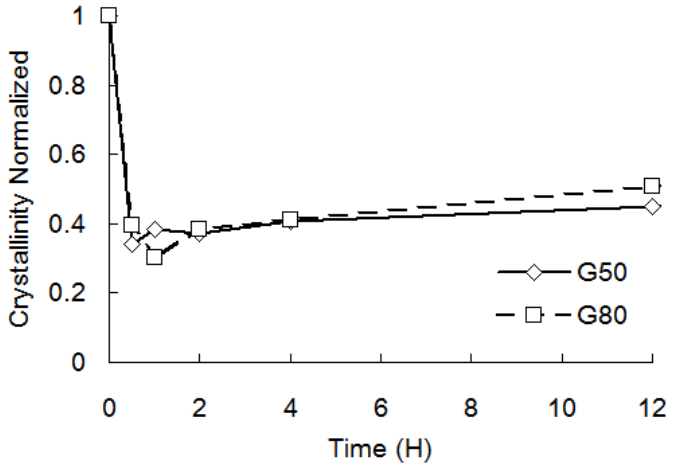

C

Fig. 4 Yang et al. International Journal of Biological Macromolecules

Fig. 4. XRD results of G50 and G80 samples after hydrothermal treatment for different time periods.

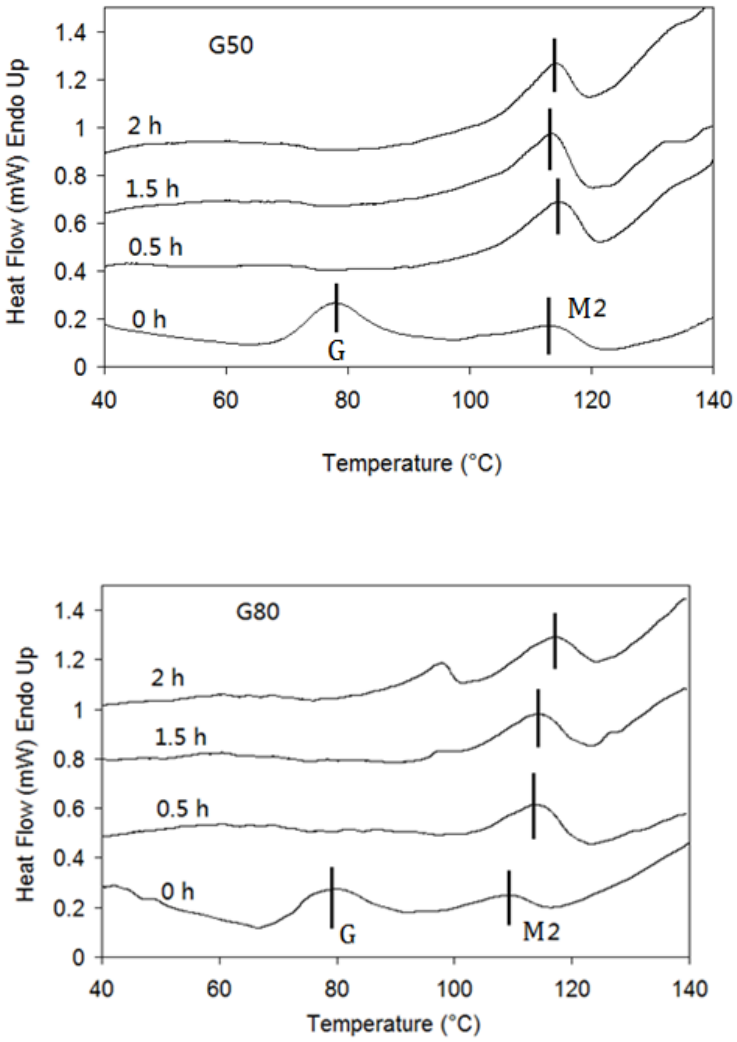

Fig. 5

Yang et al.

International Journal of Biological Macromolecules

Fig. 5. DSC results of G50 (upper) and G80 (lower) hydrothermally treated for different time periods. G (gelatinization) represents the transition from smectic to nematic phase of amylopectin double helical structure, usually overlapped with the helix-coil transition

associated with the unwinding of amylopectin double helices; M2 denotes the thermal transition associated with the unwinding of amylose single helices.

Fig. 6. Speculated model of the periphery organization of high-amylose maize starch.

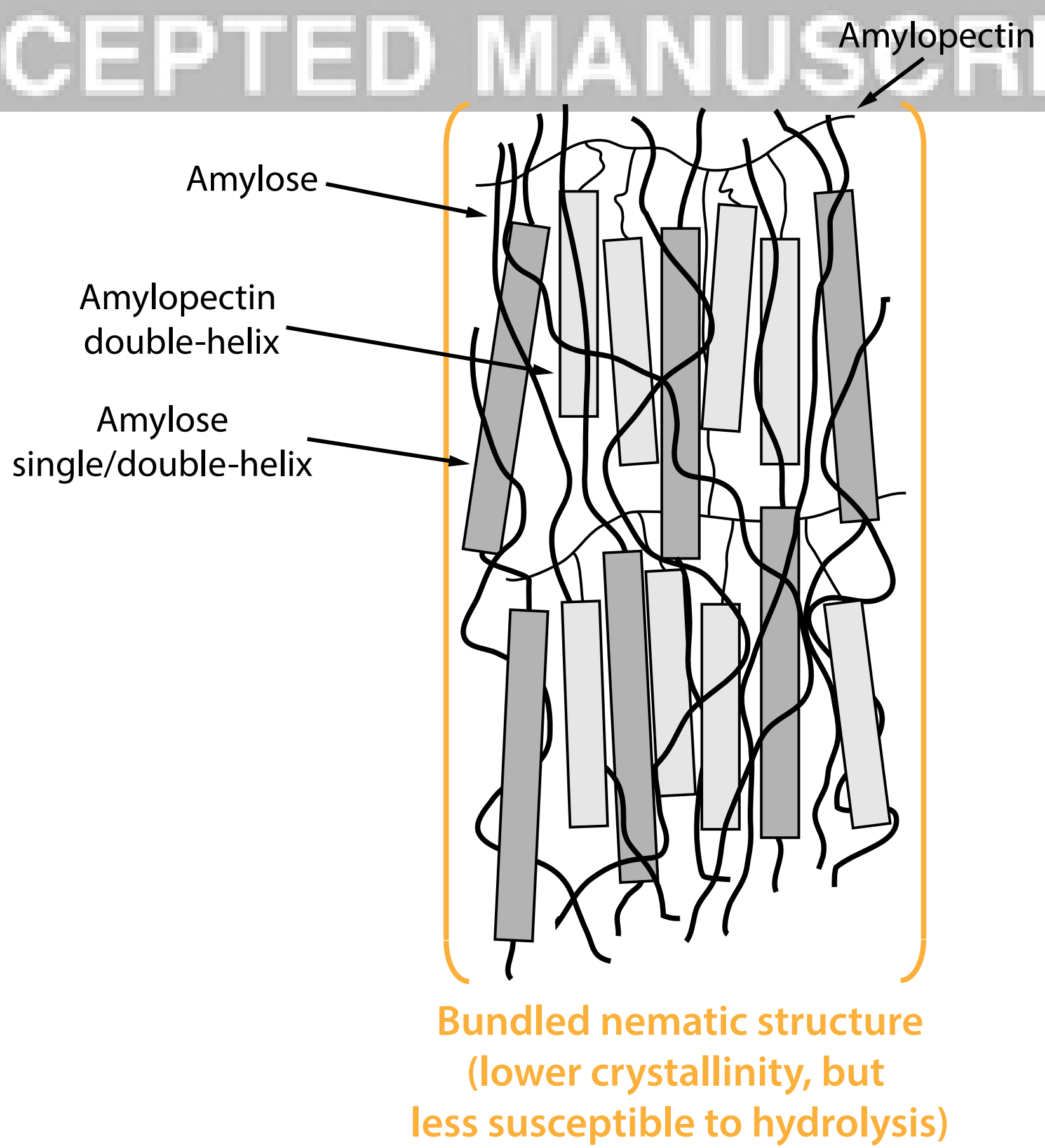

Table 1 DSC results of G50 and G80 hydrothermally treated for different time periods

Starch type	Time (h)	Peak type	T_o (°C)	T_p (°C)	ΔH (J/g)
G50	0	G	69.28	77.93	3.065
		M2	98.51	113.73	1.629
	0.5	M2	104.54	114.65	2.913
	1.5	M2	105.24	113.57	3.485
	2	M2	107.06	113.73	4.247
G80	0	G	70.76	79.27	3.051
		M2	98.93	109.1	0.955
	0.5	M2	102.37	114.15	2.322
	1.5	M2	102.99	114.15	2.412
	2	M2	103.43	116.81	2.702

Peak G and M2 correspond to the peaks in Fig. 5. T_o, T_p and ΔH are the onset temperature, peak temperature, and enthalpy of the thermal transition.